Journal of Power Sources 438 (2019) 227031

Contents lists available at ScienceDirect

Journal of Power Sources

journal homepage: www.elsevier.com/locate/jpowsour

Enhancing the organic solar cell efficiency by combining plasmonic and Förster Resonance Energy Transfer (FRET) effects

Yu Jin Jang [a,1,2], Daisuke Kawaguchi [b], Shuhei Yamaguchi [c], Sunghee Lee [a], Ju Won Lim [a,3], Heejun Kim [a], Keiji Tanaka [c,**], Dong Ha Kim [a,*]

[a] Department of Chemistry and Nano Science, Ewha Womans University, 52 Ewhayeodae-gil, Seodaemun-gu, Seoul, 03760, Republic of Korea
[b] Education Center for Global Leaders in Molecular Systems for Devices, Kyushu University, 744 Motooka Nishi-ku, Fukuoka, 819-0395, Japan
[c] Department of Applied Chemistry, Kyushu University, 744 Motooka Nishi-ku, Fukuoka, 819-0395, Japan

HIGHLIGHTS

- New approach to efficiently enhancing the organic solar cell efficiency.
- Combination of plasmonic and Förster Resonance Energy Transfer (FRET) effect.
- First demonstration of plasmonic effect in multicomponent organic solar cell devices.
- Optical and electrical demonstrations of the energy relay between light active components.
- Positive correlation of increased number of free carriers and photovoltaic efficiency.

GRAPHICAL ABSTRACT

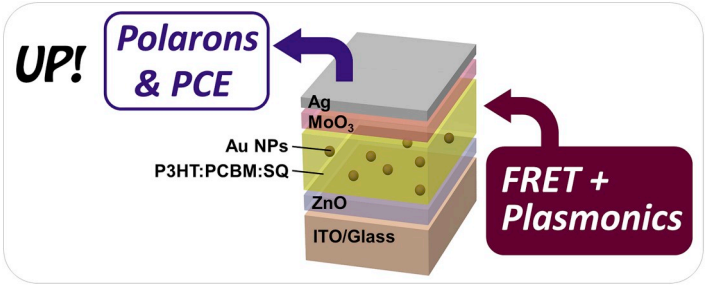

ARTICLE INFO

Keywords:
Plasmonic effect
Förster resonance energy transfer
Squaraine
Gold nanoparticles
Organic solar cells

ABSTRACT

Here, we combine two strategies i.e., Förster resonance energy transfer and plasmonic effect, to enhance the photovoltaic performance in organic solar cells by introducing gold nanoparticles and squaraine in a binary mixture of poly(3-hexylthiophene):phenyl-C_{61}-butyric acid methyl ester. In this configuration, the Förster resonance energy transfer between poly(3-hexylthiophene) and squaraine reduces the electrical loss arising from the exciton recombination in poly(3-hexylthiophene), while gold nanoparticles enable an efficient charge carrier generation in poly(3-hexylthiophene):squaraine mixture as optically confirmed by photoluminescence measurement and transient absorption spectroscopy. The multicomponent organic solar cells demonstrate an enhancement of ~36% in power conversion efficiency over the reference device.

* Corresponding author.
** Corresponding author.
E-mail addresses: k-tanaka@cstf.kyushu-u.ac.jp (K. Tanaka), dhkim@ewha.ac.kr (D.H. Kim).
[1] Center for Integrated Nanostructure Physics (CINAP), Institute for Basic Science (IBS), 2066 Seobu-ro, Jangan-gu, Suwon-si, Gyeonggi-do, 16419, Republic of Korea.
[2] Sungkyunkwan University (SKKU), 2066 Seobu-ro, Jangan-gu, Suwon-si, Gyeonggi-do, 16419, Republic of Korea.
[3] Department of Materials Science and Engineering, University of Michigan, Ann Arbor, 48109, United States.

https://doi.org/10.1016/j.jpowsour.2019.227031
Received 18 April 2019; Received in revised form 17 June 2019; Accepted 16 August 2019
Available online 22 August 2019

1. Introduction

Diverse approaches have been employed to date to achieve high power conversion efficiency (PCE) in organic solar cell (OSC) devices and they can be summarized as follows [1–4]: 1) a new polymer design with tunable highest occupied molecular orbital and lowest unoccupied molecular orbital (HOMO-LUMO) levels to increase the value of open circuit voltage (V_{OC}); 2) work function engineering of transport layers to improve the charge transfer at the interfaces, followed by an increase in the values of short circuit current (J_{SC}) and fill factor (FF); 3) the development of low-band gap polymers which extends the absorption window of solar spectrum to near infrared (NIR) region; and 4) the incorporation of multiple organic semiconductors in an active layer to realize the panchromatic sensitization as an approach for a higher value of J_{SC}.

Along with the aforementioned strategies, researchers have developed clever ways to manipulate light in photovoltaic devices by embedding plasmonic nanostructures in an active layer of OSCs [5–8]. The coupling between incident photons and the collectively oscillating electrons in colloidal plasmonic nanoparticles (NPs) generated highly energetic local electric field on the surface, acting as a light concentrator in the solar cell device. This near-field was sufficient to change the absorption and emission properties of organic sensitizers when they come close [9–15]. In addition, this plasmonic energy was efficiently transferred to the organic sensitizers within the decay length of the near-field in the presence of spectral overlap between plasmonic NPs and organic sensitizers. It significantly enhanced the number of charge carriers generated in OSC devices [5,16].

The reduction of recombination loss which resulted from a large binding energy of excitons in organic semiconductors has been also considered to ultimately achieve a high PCE [1,17]. Taylor et al. have reported that squaraine (SQ) molecules incorporated in conventional poly(3-hexylthiophene):phenyl-C_{61}-butyric acid methyl ester (P3HT:PCBM) binary bulk heterojunction solar cells generated extra excitons via Förster resonance energy transfer (FRET) [18]. Since FRET is a mechanism of a non-radiative energy transport between a pair of donor and acceptor fluorophores placed in close proximity within ~10 nm and the FRET efficiency is primarily governed by the spectral overlap between donor and acceptor materials [19], the excitation of SQ by the emission from P3HT resulted in the improvement in PCE by up to ~38% over the reference device due to the increase in J_{SC} and FF values.

Herein, we boost the light utilization in OSCs by combining the FRET and plasmonic effect. To this end, SQ and Au NPs were simultaneously incorporated into the binary mixture of P3HT:PCBM layer as depicted in Fig. 1a. In this scheme (Fig. 1b), SQ dyes generate extra charge carriers in the device via FRET and plasmonic nanostructures enhance the photoconversion into free charge carriers in P3HT:SQ via multiple plasmonic effect including near-field enhancement, plasmon resonant energy transfer and plasmonic hot carrier injection. It led to an enhancement of ~36% in PCE of a multicomponent OSC device over the reference device.

2. Experimental section

2.1. Synthesis of Au NPs

Au NPs were synthesized as follows [20]. First, Au precursor solution was prepared by dissolving 50 mg of $HAuCl_4$ in the mixture of 1 mL toluene and 1.2 mL oleylamine (OA). When the mixture solution of 49 mL toluene and 2.9 mL OA started boiling, the Au precursor was injected to the solution and it remained for 2 h at the same temperature with a vigorous stirring. After cooling down, 15 mL of Au NP solution was mixed with 30 mL of methanol. The precipitated Au NPs were washed with methanol three times by centrifugation and then dried completely before use. Finally, Au NPs were redispersed into 1 mL of anhydrous 1,2-dichlorobenzene (DCB).

2.2. Preparation of binary, ternary or quaternary active materials

For binary active material (P3HT:PCBM), 15 mg of P3HT and 15 mg of PCBM were mixed in 1 mL of DCB for 3 h at 70 °C. For ternary mixture (P3HT:PCBM:SQ), 2 mg of SQ was separately stirred vigorously in 1 mL of DCB at least for 6 h and the solutions of SQ and P3HT:PCBM were mixed inside the N_2 gas purged glove box with a ratio of 10:90 (w/w). For quaternary system (P3HT:PCBM:SQ:Au), 2 μL of Au NP dispersion in DCB was added to P3HT:PCBM:SQ solution in the glove box. In order to

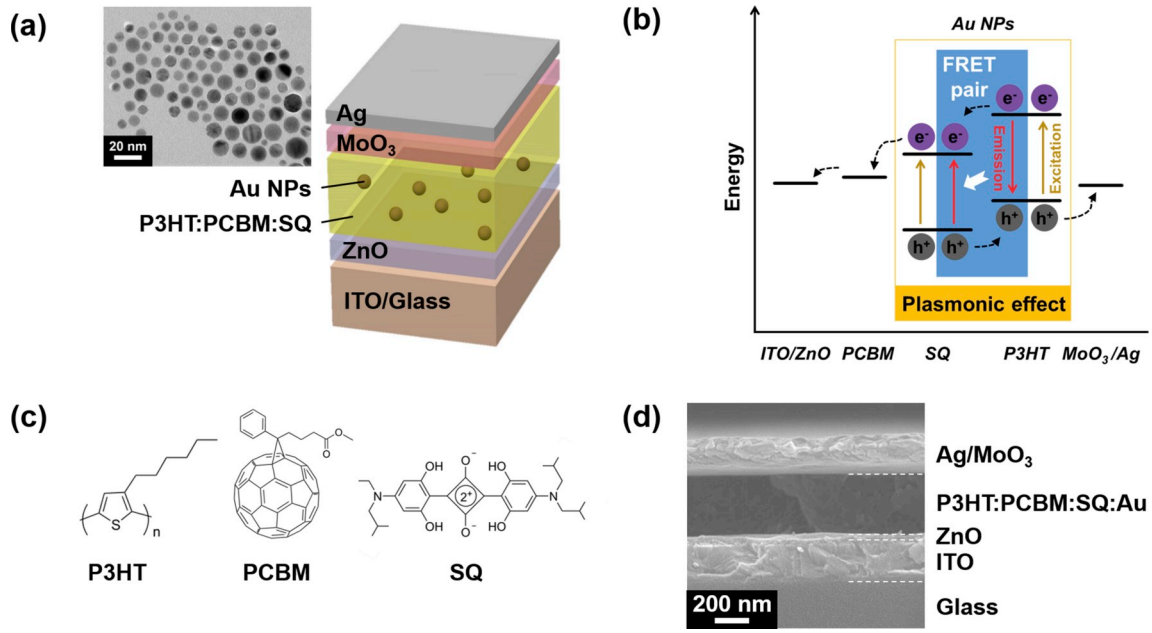

Fig. 1. (a) Schematic illustration of an OSC device with a blend film of P3HT:PCBM with additional SQ molecules and Au NPs. TEM image of Au NPs is presented on the left side. (b) Working mechanism of plasmonic FRET OSCs. (c) Chemical structures of P3HT, PCBM and SQ. (d) Cross-sectional SEM image of a plasmonic FRET OSC device.

obtain the same film thicknesses, we adjusted the solution concentration of all the active materials to be equal to quaternary solution by adding a portion of DCB to binary or ternary mixtures.

2.3. Preparation of active material thin films for optical measurement

Since PCBM rapidly accepts charge carriers from P3HT and reduces the photoluminescence (PL) intensity as well as transient absorption spectroscopy (TAS) signals of P3HT, it was excluded from the samples for optical measurement. Thus, solutions of neat P3HT, P3HT:Au, P3HT:SQ and P3HT:SQ:Au were prepared and spin-coated on glass or quartz substrates. The mixing protocols for P3HT, P3HT:SQ and P3HT:SQ:Au were same with that described in 2.2. but without PCBM. For P3HT:Au case, 2 μL of Au NP dispersion in DCB was added to P3HT solution and stirred for 2 h before spin-coating.

2.4. OSC fabrication

Indium tin oxide (ITO) substrates were sequentially cleaned in acetone and isopropanol in a sonication bath, and then with the fume of boiling isopropanol. ZnO sol-gel solution was prepared by mixing 0.1 g of zinc acetate, 10 mL of 2-methoxyethanol and 0.28 mL of ethanolamine. The mixture was stirred for 24 h. After the oxygen plasma treatment, 200 μL of ZnO sol-gel solution was dropped onto 2.5 cm x 2.5 cm patterned ITO substrate and then spin-coated at 2400 rpm for 60s, followed by thermal annealing at 150 °C for 1 h. Binary, ternary and quaternary solutions of active material were spin-coated at 500 rpm for 5s and at 900 rpm for 5s in N_2 purged glove box onto the ZnO coated ITO substrates. After that, the active layers were naturally dried and thermal-annealed on a hot plate at 150 °C for 20 min. Finally, MoO_3 and Ag layers were thermally evaporated. The active cell area of the OSC devices was 0.06 cm^2.

2.5. Instruments and characterization

Tapping mode atomic force microscopy (AFM) images were obtained by Veeco D3100. Scanning electron microscope (SEM) and transmission electron microscopy (TEM) measurements were performed using JEOL JSM-6700F and JEOL JSM-2100-F, respectively. Absorption and emission properties of active materials were investigated by Cary 5000, Varian, Inc. and LS55, PerkinElmer, respectively. Femtosecond pump-probe TAS system was composed of a transient absorption spectrometer (Ultrafast Systems, Helios) and a regenerative amplified Ti:sapphire laser (Spectra-Physics, Solstice). More details on TAS measurement can be found in our previous reports [21,22]. The wavelength and intensity of the pump laser were 400 nm and 0.2 W, respectively. The transient absorption spectra were recorded at RT as a function of time from ~5 to 100 ps. The current density-voltage (J–V) profiles were measured under AM 1.5G illumination at 100 mW/cm^2 using Keithley 2400 solar cell I–V measurement system.

3. Results and discussion

3.1. Major components in OSC devices

In this study, Au nanospheres with a size of 8.41 ± 2.15 nm were synthesized in toluene and redispersed in DCB (TEM image in Fig. 1a). The molecular structures of P3HT, PCBM and SQ are displayed in Fig. 1c. The device configuration was confirmed by cross-sectional SEM image in Fig. 1d. The thickness of ZnO, active material and MoO_3/Ag layers was approximately ~40 nm, ~300 nm and ~200 nm, respectively.

3.2. Optical properties of active materials in OSC devices

The optical properties of Au NPs, P3HT and SQ were characterized by UV–Vis spectrometer and Fig. 2a shows that Au NP dispersion in DCB exhibited a localized surface plasmon resonance (LSPR) band with the maximum peak at 533 nm (pink line), which is well matched with the absorption band of P3HT (black line). This implies that Au NPs would efficiently modulate the optical properties of P3HT.

Steady-state PL spectra in Fig. 2b was obtained under the excitation wavelength of 525 nm to monitor the change in the emission properties of P3HT and neat P3HT film exhibited PL peaks over 600–800 nm as shown in Fig. 2b (black line). In our case, the absorption band of SQ at 640 nm (blue line in Fig. 2a) is well matched with the emission band of P3HT and the excitation of SQ by the recombination loss caused by P3HT via FRET is highly expected. Indeed, large decrease in PL intensity was observed for P3HT:SQ films (Fig. 2b, blue line) presumably due to FRET from P3HT to SQ [18]. PL measurement also reveals that the incorporation of Au NPs in P3HT film significantly increased the PL intensity of P3HT by up to 55.8% (Fig. 2b, green line) and the PL intensity was also enhanced by up to 19% when Au NPs were embedded into a FRET pair, i.e., P3HT:SQ blend (Fig. 2, pink line). It indicates that plasmonic effect appeared not only in neat P3HT film but also in P3HT:SQ blend system. It has been reported that the dipole-dipole coupling between Au NPs and P3HT gives the same effect with the photoexcitation in the high power regime and creates more charge carriers useful for the enhancement of photocurrent [9–14]. Thus, the enhancement of PL intensity after the incorporation of Au NPs can be understood by the increased number of charge carriers in active layers [13,23,24].

3.3. Monitoring of the photo-induced charge carriers in P3HT by TAS

Femtosecond pump-probe TAS measurement was conducted to

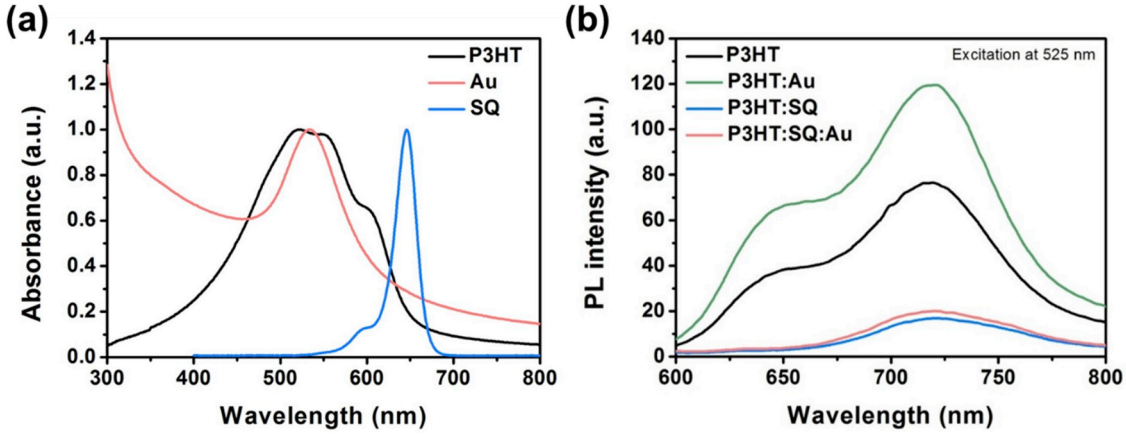

Fig. 2. (a) Normalized absorption spectra of P3HT thin film, Au NPs and SQ. (b) PL spectra of thin layers of P3HT, P3HT:Au, P3HT:SQ and P3HT:SQ:Au.

specifically monitor the formation of photo-induced charge carriers in P3HT. Pump wavelength was fixed at 400 nm and the intensity of pump laser was set at 0.2 W to avoid the direct formation of polarons (**P**) from hot-excitons [21,22]. TAS data for all samples are summarized in the Supplementary Information (Fig. S1-4 and Table S1-4).

The optical density (ΔOD) for singlet excitons (**S**), polaron pairs (**PP**) and polarons (**P**) from TA spectra were extracted on the basis of a curve-fitting analysis. The decay times for **S** and **PP** were obtained from Equation (1),

$$\Delta OD = \sum_{i=1}^{n} A_i \exp\left(-\frac{t}{\tau_i}\right) \quad (1)$$

where A_i and τ_i are pre-exponential factor and time constant for the ith decay process, and n is the number of decays involved. Similarly, the rise time for **P** was obtained from Equation (2),

$$\Delta OD = \sum_{i=1}^{n}\left(-A_i \exp\left(-\frac{t}{\tau_i}\right)\right) + b \quad (2)$$

where b is an asymptotic ΔOD value at 50 ps. The average decay or rise time (τ_{ave}) was given by Equation (3),

$$\tau_{ave} = \sum_{i=1}^{n} A_i \tau_i \quad (3)$$

The details on analyses are also described in the Supplementary Information.

We found that Au NPs in the P3HT and P3HT:SQ layer rarely affected the initial ΔOD value at the time of 0 as well as the decay of **S** (τ_{ave}(**S**)$_{P3HT}$ and τ_{ave}(**S**)$_{P3HT:AuNP}$: 17 and 15 ps, respectively) as shown in the time dependence of ΔOD for **S** of Fig. 3a. Although our result indicated that the inclusion of Au NPs in P3HT and P3HT:SQ did not contribute to the increase in the number density of **S** at 1100 nm, Figs. S1a–4a and Figs. S1c–4c show that ΔOD for **PP** at 650 nm was apparently increased in the presence of Au NPs as confirmed with TAS by other groups as well [25,26]. In addition, ΔOD for **P** at 1000 nm was remarkably increased by incorporating Au NPs in P3HT and P3HT:SQ (Fig. 3b) and the magnitude of **P** at the time of 0 was much higher in P3HT and P3HT:SQ with Au NPs than those without Au NPs (Figs. S1b–4b). This points out that Au NPs in P3HT and P3HT:SQ acted as a promoter to generate free charge carriers rather than being traps to facilitate the recombination [25,27].

Although plasmon resonant energy transfer would be the dominant factor to affect the yield of **S**, **PP** and **P** rather than plasmonic hot carrier injection in our case when considering the unfavorable geometry of Au NPs [28], it can be plausible to take into account of the contribution of plasmonic hot carriers to interpret the unexpected increase in **P** in P3HT or P3HT:SQ. Plasmonic hot carriers such as hot electrons and holes are created by the plasmon excitation and they can be transferred to an adjacent medium such as metal oxides, organic molecules and P3HT within 100 fs time scale [28–33]. In most cases, hot electrons with a higher energy above the height of Schottky barrier are moved from metal to the conduction band of semiconductors at the interface. However, Xiang et al. found that hot electrons were directly transferred from the Fermi level of Au to the LUMO of P3HT and separated into free charge carriers within ~150 fs when P3HT solution was spin-coated on Au substrate [30]. Strein et al. also confirmed that the transfer of hot holes from PbS to P3HT increased the photoinduced absorption (PIA) signal which corresponds to **P** at the sub-ps time scale [33]. In addition, Reineck et al. demonstrated that plasmonic hot carriers were transferred by tunnelling from Au NPs to TiO_2 across SiO_2 with a thickness of 2–4 nm and it apparently contributed to the photocurrent in dye-sensitized solar cells [34]. The Au@SiO_2@TiO_2 system in the previous study is quite similar to our P3HT:Au or P3HT:SQ:Au, which are spaced by OA with the length of alkyl chains of ~2 nm [35,36] between Au NPs and polymers. All the above findings from TAS results in Fig. 3b led us to conclude that hot electron injection from Au NPs to P3HT or P3HT:SQ as well as plasmon resonant energy transfer between the light active components resulted in the remarkable increase in **P**.

Fig. 3a also reveals that the initial ΔOD value at the time of 0 was insensitive to the addition of SQ into P3HT. This implies that the initial **S** concentration of P3HT right after the excitation process was not associated with the inclusion of SQ. However, the **S** decay was accelerated by SQ and the τ_{ave}(**S**)$_{P3HT:SQ}$ value was decreased from 17 to 8 ps, which is most likely that the energy transfer from P3HT to SQ via FRET is related to the event. Although Au NPs were present in P3HT:SQ, the **S** decay was slightly decreased (5.6 ps), indicating that Au NP does not apparently impact on FRET from P3HT to SQ, unlike the situations observed in previous studies [37,38]. However, τ(**P**) became smaller when Au NPs or SQ were added into the system as shown in Fig. 3b. The smallest value was obtained in the presence of both Au NPs and SQ in P3HT. These results make it clear that the formation of photo-induced charge carriers in P3HT is synergistically enhanced by the combination of FRET and plasmonic effect.

3.4. Solar cell performances

As shown in Fig. 4, J-V profiles were obtained from OSC devices including a thin layer of P3HT:PCBM, P3HT:PCBM:SQ or P3HT:PCBM:SQ:Au as an active layer and the observed photovoltaic parameters are summarized in the inset table in Fig. 4. Compared with a typical P3HT:PCBM binary case, an OSC device with ternary blend system (P3HT:PCBM:SQ) exhibited a higher PCE value by 12.6% due to the enhancement of J_{SC}. Surprisingly, the introduction of Au NPs into P3HT:PCBM:SQ resulted in a significant enhancement in J_{SC} and FF values. As a result, the PCE value of quaternary OSC device exhibited the maximum enhancement of 20.7 and 36% compared with ternary and binary OSC devices, respectively. This clearly demonstrates that the optical gain in

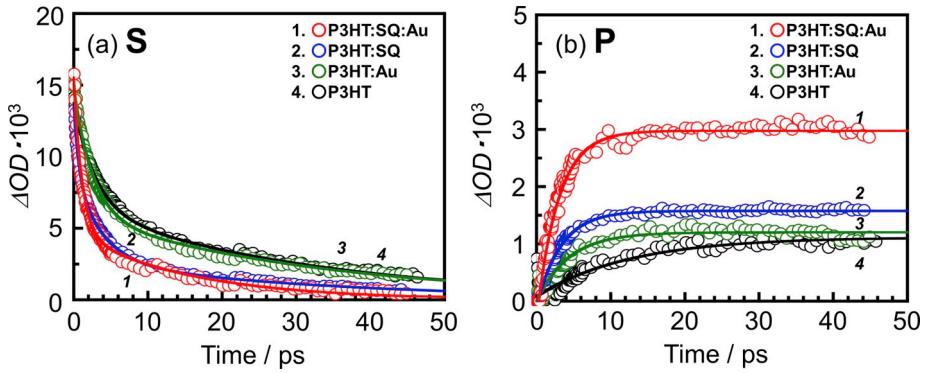

Fig. 3. Time dependence of ΔOD for (a) **S** and (b) **P** in P3HT, P3HT:Au, P3HT:SQ and P3HT:SQ:Au. Symbols and solid lines denote experimental data and the fitting results, respectively.

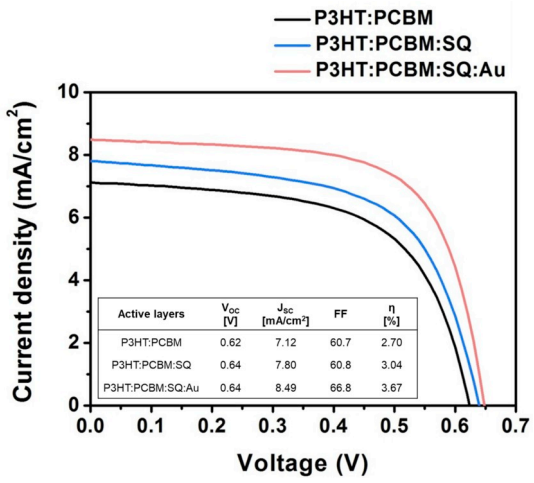

Fig. 4. J-V curves obtained from OSCs consisting of P3HT:PCBM, P3HT:PCBM:SQ or P3HT:PCBM:SQ:Au active materials. Summary of the photovoltaic parameters of the OSC devices in Fig. 4 are presented in the inset table.

P3HT by plasmonic effect contributed to the number of charge carriers converted into PCE of OSC devices.

Other than FRET effect, broadband absorption due to the inclusion of two different organic sensitizers might be one possible explanation for the enhancement of PCE in ternary system [2,18]. In this study, we incorporated both P3HT and SQ in one device. Thus, the absorption range of the ternary OSC device was extended to ~700 nm. That resulted in a better photon harvesting in the OSC device, leading to an improvement of J_{SC} value [2,18]. In addition, based on the LUMO levels of P3HT, SQ and PCBM which correspond to approximately 3, 3.5 and 4 eV, a better electron transfer from P3HT to PCBM could be achieved after the incorporation of SQ, generating a cascade type of energy band alignment [2,18]. This also can contribute to higher J_{SC} and FF values. V_{OC} value is defined as an energy gap between HOMO and LUMO levels of organic sensitizers and fullerene derivatives, respectively. The HOMO level of SQ is located in between that of P3HT and PCBM [18,39]. It accounts for a slight increase in V_{OC} of FRET OSC device over the reference value. Fig. S5 shows the AFM images of P3HT, P3HT:SQ and P3HT:SQ:Au films. The values of root-mean-square (RMS) roughness were obtained from the height images and they are summarized in Table S5. Neat P3HT film exhibited the highest RMS value and it was decreased after the incorporation of SQ into P3HT but a bit increased by Au NPs. It is well known that smoother film is advantageous for the charge transfer at the interface between the active layer and electrodes [40]. The alteration in the surface morphology can be another factor to enhance the PCE of ternary and quaternary OSCs over the reference device.

The enhancement of PCE by up to ~36% in plasmonic FRET OSC device is quite noticeable when we consider that the improvement of PCE values by plasmonic effect in conventional binary OSC devices has been limited to a level of ~20% [5]. This observation again confirms that our approach to combining FRET and plasmonic effect in one device has a positive impact on solar cell performance.

4. Conclusion

Our approach to improving the PCE by exploiting both plasmonic and FRET effect demonstrated its feasibility in OSCs. As confirmed by PL, TAS and photovoltaic performances, FRET occurred in between P3HT and SQ and Au NPs boosted the number of free charge carriers in FRET OSC device. Further improvement in PCE may be achievable by incorporating plasmonic nanostructures with different composition, shape and size because such parameters can tune the optical properties of plasmonic nanostructures and manipulate the solar-to-electrical conversion efficiency of OSC devices.

Acknowledgements

This work was supported by National Research Foundation of Korea Grant funded by the Korean Government (2015M1A2A2058365; 2017R1A2A1A05022387; 2018M3D1A1058536) and by the Korea Institute of Energy Technology Evaluation and Planning (KETEP) Grant funded by the Korean Government (MOTIE) (No. 20173010013340).

Appendix A. Supplementary data

Supplementary data to this article can be found online at https://doi.org/10.1016/j.jpowsour.2019.227031.

References

[1] G. Li, R. Zhu, Y. Yang, Polymer solar cells, Nat. Photonics 6 (2012) 153–161. https://doi.org/10.1038/nphoton.2012.11.
[2] T. Ameri, P. Khoram, J. Min, C.J. Brabec, Organic ternary solar cells: a review, Adv. Mater. 25 (2013) 4245–4266. https://doi.org/10.1002/adma.201300623.
[3] Y. Yang, W. Chen, L. Dou, W.-H. Chang, H.-S. Duan, B. Bob, G. Li, Y. Yang, High-performance multiple-donor bulk heterojunction solar cells, Nat. Photonics 9 (2015) 190–198. https://doi.org/10.1038/NPHOTON.2015.9.
[4] H.-Y. Chen, J. Hou, S. Zhang, Y. Liang, G. Yang, Y. Yang, L. Yu, Y. Wu, G. Li, Polymer solar cells with enhanced open-circuit voltage and efficiency, Nat. Photonics 3 (2009) 649–653. https://doi.org/10.1038/nphoton.2009.192.
[5] Y. Jang, Y. Jang, S. Kim, L. Quan, K. Chung, D. Kim, Plasmonic solar cells: from rational design to mechanism overview, Chem. Rev. 116 (2016) 14982–15034. https://doi.org/10.1021/acs.chemrev.6b00302.
[6] Q. Gan, F.J. Bartoli, Z.H. Kafafi, Plasmonic-enhanced organic photovoltaics: breaking the 10% efficiency barrier, Adv. Mater. 25 (2013) 2385–2396. https://doi.org/10.1002/adma.201203323.
[7] E. Stratakis, E. Kymakis, Nanoparticle-based plasmonic organic photovoltaic devices, Mater. Today 16 (2013) 133–146. http://www.sciencedirect.com/science/article/pii/S1369702113001065.
[8] E.S. Arinze, B. Qiu, G. Nyirjesy, S.M. Thon, Plasmonic nanoparticle enhancement of solution-processed solar cells: practical limits and opportunities, ACS Photonics 3 (2016) 158–173. https://doi.org/10.1021/acsphotonics.5b00428.
[9] J.-L. Wu, F.-C. Chen, Y.-S. Hsiao, F.-C. Chien, P. Chen, C.-H. Kuo, M.H. Huang, C.-S. Hsu, Surface plasmonic effects of metallic nanoparticles on the performance of polymer bulk heterojunction solar cells, ACS Nano 5 (2011) 959–967. https://doi.org/10.1021/nn102295p.
[10] T.Z. Oo, N. Mathews, G. Xing, B. Wu, B. Xing, L.H. Wong, T. Sum, S.G. Mhaisalkar, Ultrafine gold nanowire networks as plasmonic antennae in organic photovoltaics, J. Phys. Chem. C 116 (2012) 6453–6458. https://doi.org/10.1021/jp2099637.
[11] M.-K. Chuang, S.-W. Lin, F.-C. Chen, C.-W. Chu, C.-S. Hsu, Gold nanoparticle-decorated graphene oxides for plasmonic-enhanced polymer photovoltaic devices, Nanoscale 6 (2013) 1573–1579. https://doi.org/10.1039/c3nr05077g.
[12] N. Chaturvedi, S. Swami, V. Dutta, Plasmonic effect of spray-deposited Au nanoparticles on the performance of inverted organic solar cells, Nanoscale 6 (2014) 10772–10778. https://doi.org/10.1039/c4nr03270e.
[13] J. Lee, J. Lim, N. Lee, H. Park, K. Lee, T. Jeon, S. Nam, J. Kim, J. Shin, S. Kim, Synergistic concurrent enhancement of charge generation, dissociation, and transport in organic solar cells with plasmonic metal–carbon nanotube hybrids, Adv. Mater. 27 (2015) 1519–1525. https://doi.org/10.1002/adma.201404248.
[14] M.-K. Chuang, F.-C. Chen, Synergistic plasmonic effects of metal nanoparticle–decorated PEGylated graphene oxides in polymer solar cells, ACS Appl. Mater. Interfaces 7 (2015) 7397–7405. https://doi.org/10.1021/acsami.5b01161.
[15] D. Zheng, X. Pang, M. Wang, Y. He, C. Lin, Z. Lin, Unconventional route to hairy plasmonic/semiconductor core/shell nanoparticles with precisely controlled dimensions and their use in solar energy conversion, Chem. Mater. 27 (2015) 5271–5278. https://doi.org/10.1021/acs.chemmater.5b01422.
[16] W.R. Erwin, H.F. Zarick, E.M. Talbert, R. Bardhan, Light trapping in mesoporous solar cells with plasmonic nanostructures, Energy Environ. Sci. 9 (2016) 1577–1601. https://doi.org/10.1039/c5ee03847b.
[17] J.D. Servaites, M.A. Ratner, T.J. Marks, Organic solar cells: a new look at traditional models, Energy Environ. Sci. 4 (2011) 4410–4422. https://doi.org/10.1039/C1EE01663F.
[18] J.-S. Huang, T. Goh, X. Li, M.Y. Sfeir, E.A. Bielinski, S. Tomasulo, M.L. Lee, N. Hazari, A.D. Taylor, Polymer bulk heterojunction solar cells employing Förster resonance energy transfer, Nat. Photonics 7 (2013) 479–485. https://doi.org/10.1038/nphoton.2013.82.
[19] P.R. Selvin, The renaissance of fluorescence resonance energy transfer, Nat. Struct. Mol. Biol. 7 (2000) 730–734. https://doi.org/10.1038/78948.
[20] H. Hiramatsu, F.E. Osterloh, A simple large-scale synthesis of nearly monodisperse gold and silver nanoparticles with adjustable sizes and with exchangeable surfactants, Chem. Mater. 16 (2004) 2509–2511. https://doi.org/10.1021/cm049532v.

[21] Y. Ogata, D. Kawaguchi, K. Tanaka, An effect of molecular motion on carrier formation in a poly(3-hexylthiophene) film, Sci. Rep. 5 (2015) 8436. https://doi.org/10.1038/srep08436.
[22] Y. Ogata, D. Kawaguchi, K. Tanaka, The impact of polymer dynamics on photoinduced carrier formation in films of semiconducting polymers, J. Phys. Chem. Lett. 6 (2015) 4794–4798. https://doi.org/10.1021/acs.jpclett.5b02255.
[23] H.I. Park, S. Lee, J.M. Lee, S.A. Nam, T. Jeon, S.W. Han, S.O. Kim, High performance organic photovoltaics with plasmonic-coupled metal nanoparticle clusters, ACS Nano 8 (2014) 10305–10312. https://doi.org/10.1021/nn503508p.
[24] D.C. Lim, B.Y. Seo, S. Nho, D.H. Kim, E.M. Hong, J.Y. Lee, S.-Y. Park, C.-L. Lee, Y. D. Kim, S. Cho, Emissive nanoclusters based on subnanometer-sized Au38 cores for boosting the performance of inverted organic photovoltaic cells, Adv. Energy Mater. 5 (2015) 1500393. https://onlinelibrary.wiley.com/doi/abs/10.1002/aenm.201500393.
[25] P. Du, P. Jing, D. Li, Y. Cao, Z. Liu, Z. Sun, Plasmonic Ag@Oxide nanoprisms for enhanced performance of organic solar cells, Small 11 (2015) 2454–2462. https://onlinelibrary.wiley.com/doi/abs/10.1002/smll.201402757.
[26] H. Wang, H.-Y. Wang, B.-R. Gao, Y. Jiang, Z.-Y. Yang, Y.-W. Hao, Q.-D. Chen, X.-B. Du, H.-B. Sun, Surface plasmon enhanced absorption dynamics of regioregular poly(3-hexylthiophene), Appl. Phys. Lett. 98 (2011) 251501. https://aip.scitation.org/doi/abs/10.1063/1.3590728.
[27] B. Wu, X. Wu, C. Guan, K. Fai Tai, E.K.L. Yeow, H. Jin Fan, N. Mathews, T.C. Sum, Uncovering loss mechanisms in silver nanoparticle-blended plasmonic organic solar cells, Nat. Commun. 4 (2013) (2004). https://doi.org/10.1038/ncomms3004.
[28] S.K. Cushing, J. Li, J. Bright, B.T. Yost, P. Zheng, A.D. Bristow, N. Wu, Controlling plasmon-induced resonance energy transfer and hot electron injection processes in metal@TiO_2 core–shell nanoparticles, J. Phys. Chem. C 119 (2015) 16239–16244. https://doi.org/10.1021/acs.jpcc.5b03955.
[29] M.L. Brongersma, N.J. Halas, P. Nordlander, Plasmon-induced hot carrier science and technology, Nat. Nanotechnol. 10 (2015) 25. https://doi.org/10.1038/nnano.2014.311.
[30] B. Xiang, Y. Li, C.H. Pham, F. Paesani, W. Xiong, Ultrafast direct electron transfer at organic semiconductor and metal interfaces, Sci. Adv. 3 (2017) e1701508, http://advances.sciencemag.org/content/advances/3/11/e1701508.full.pdf.
[31] Y.J. Jang, K. Chung, J.S. Lee, C.H. Choi, J.W. Lim, D.H. Kim, Plasmonic hot carriers imaging: promise and outlook, ACS Photonics 5 (2018) 4711–4723. https://doi.org/10.1021/acsphotonics.8b01021.
[32] D.C. Ratchford, A.D. Dunkelberger, I. Vurgaftman, J.C. Owrutsky, P.E. Pehrsson, Quantification of efficient plasmonic hot-electron injection in gold nanoparticle–TiO_2 films, Nano Lett. 17 (2017) 6047–6055. https://doi.org/10.1021/acs.nanolett.7b02366.
[33] E. Strein, D.W. deQuilettes, S.T. Hsieh, A.E. Colbert, D.S. Ginger, Hot hole transfer increasing polaron yields in hybrid conjugated polymer/PbS blends, J. Phys. Chem. Lett. 5 (2014) 208–211. https://doi.org/10.1021/jz402383x.
[34] P. Reineck, G.P. Lee, D. Brick, M. Karg, P. Mulvaney, U. Bach, A solid-state plasmonic solar cell via metal nanoparticle self-assembly, Adv. Mater. 24 (2012) 4750–4755. https://onlinelibrary.wiley.com/doi/abs/10.1002/adma.201200994.
[35] J. Xie, C. Xu, N. Kohler, Y. Hou, S. Sun, Controlled PEGylation of monodisperse Fe_3O_4 nanoparticles for reduced non-specific uptake by macrophage cells, Adv. Mater. 19 (2007) 3163–3166. https://onlinelibrary.wiley.com/doi/abs/10.1002/adma.200701975.
[36] X. Lu, M.S. Yavuz, H.-Y. Tuan, B.A. Korgel, Y. Xia, Ultrathin gold nanowires can be obtained by reducing polymeric strands of oleylamine−AuCl complexes formed via aurophilic interaction, J. Am. Chem. Soc. 130 (2008) 8900–8901. https://doi.org/10.1021/ja803343m.
[37] L. Zhao, T. Ming, L. Shao, H. Chen, J. Wang, Plasmon-controlled Förster resonance energy transfer, J. Phys. Chem. C 116 (2012) 8287–8296. https://doi.org/10.1021/jp300916a.
[38] X. Zhang, C.A. Marocico, M. Lunz, V.A. Gerard, Y.K. Gun'ko, V. Lesnyak, N. Gaponik, A.S. Susha, A.L. Rogach, L.A. Bradley, Experimental and theoretical investigation of the distance dependence of localized surface plasmon coupled förster resonance energy transfer, ACS Nano 8 (2014) 1273–1283. https://doi.org/10.1021/nn406530m.
[39] G. Wei, X. Xiao, S. Wang, K. Sun, K.J. Bergemann, M.E. Thompson, S.R. Forrest, Functionalized squaraine donors for nanocrystalline organic photovoltaics, ACS Nano 6 (2012) 972–978. https://doi.org/10.1021/nn204676j.
[40] M. Zhu, H. Kim, Y.J. Jang, S. Park, D.Y. Ryu, K. Kim, P. Tang, F. Qiu, D.H. Kim, J. Peng, Toward high efficiency organic photovoltaic devices with enhanced thermal stability utilizing P3HT-*b*-P3PHT block copolymer additives, J. Mater. Chem. 4 (2016) 18432–18443. https://doi.org/10.1039/C6TA08181A.